RSC Advances

PAPER

View Article Online
View Journal | View Issue

Cite this: *RSC Adv.*, 2020, **10**, 25696

Nonlinear photoresponse of $NaYF_4$:Yb,Er@$NaYF_4$ nanocrystals under green CW excitation: a comprehensive study†

Nahid Ghazyani,[ab] Mohammad Hossein Majles Ara *[ab] and Mohammad Raoufi[cd]

One of the efficient and well-known upconverting nanomaterials is $NaYF_4$:Yb,Er@$NaYF_4$, which emits photoluminescence at 545 nm and 660 nm under an excitation of 980 nm. Here, the nonlinearity of β-$NaYF_4$:Yb,Er@$NaYF_4$ at 532 nm is investigated using three nonlinear approaches. For the first time, the nonlinear optical conjugation of $NaYF_4$:Yb,Er@$NaYF_4$ nanocrystals is observed using the degenerate four-wave mixing method. In the optical bistability study, the optical hysteresis of $NaYF_4$:Yb,Er@$NaYF_4$ is measured using the Mach–Zehnder interferometer nonlinear ring cavity, and the results of bistability loops show different behaviors at different power regimes. Finally, the *Z*-scan technique is used for determining the nonlinear absorption and refraction coefficients, which are calculated in the order of 10^{-4} (cm W^{-1}) and 10^{-8} (cm^2 W^{-1}), respectively. The results indicate that by increasing incident powers, optical behaviour changes in both optical bistability and *Z*-scan. Therefore, the results exhibit that the β-$NaYF_4$:Yb,Er@$NaYF_4$ nanocrystals have nonlinear photoresponses at both 980 and 532 nm, which could be promising for photonic devices based on NIR light and visible light.

Received 12th February 2020
Accepted 3rd June 2020

DOI: 10.1039/d0ra01380c

rsc.li/rsc-advances

Introduction

Nonlinear optical (NLO) properties are observed when NLO materials are excited under high-intensity laser light.[1] NLO materials have reported many applications in photonic devices and NLO applications have been studied in different materials, especially for inorganic complexes. However, these materials have several practical problems such as photo and thermal damaging, which limit their applications.[2] In this regard, lanthanide-doped upconversion nanoparticles (UCNPs) are an emerging type of NLO materials that appear to be the most promising candidates that could overcome such limitations due to their unique optical responses, high optical quality, stability in media without photo damage and simple coating at both lab and large scale.[3,4] However, fluorophore materials are excited at shorter wavelengths and emit at longer wavelengths;[5,6] the most important properties of UCNPs is emission in the visible region when excited under NIR wavelengths. This phenomenon is naturally a nonlinear process.[7] Generally, in processes based on anti-Stokes wavelength shifting, such as second harmonic generation (SHG) and two-photon absorption (TPA), high-power laser excitation is needed.[8] However, anti-Stokes wavelength shifting for UCNPs appears even at low-intensity excitations. At present, based on interesting properties of UCNPs, there are various applications such as laser materials,[9] photolithography,[10] optical switching,[11] nanophotonic energy storage,[12] imaging[13] and bio detections.[14] Many studies on UCNPs have focused on nonlinear processes under different NIR excitations.[15,16] The investigation of the nonlinearity of these materials at different wavelengths could be beneficial and result in multi-functional photonic devices. Because $NaYF_4$:Yb,Er@$NaYF_4$ is one of the most efficient UCNPs,[17] in this research, we first investigated wavelength shifting and the upconversion process of β-$NaYF_4$:Yb,Er@$NaYF_4$ under a CW laser of 980 nm, and then we determine non-linear photoresponse of a upconversion system by a unique approach. Since the non-linear behavior is measured using absorbance, this approach could be implemented to other energy states of Yb/Er upconversion system that does not necessarily emit light but participate in the upconversion process. Thus we focused on the optical nonlinearity of $NaYF_4$:Yb,Er@$NaYF_4$ and the investigation of its behavior under the excitation of a CW laser of 532 nm. For this purpose, three specific optical set-ups were designed: (1) Mach–Zehnder interferometer ring cavity for optical bistability study, (2) degenerate four-wave mixing set-up used for optical phase conjugation observation, and (3) open aperture and close aperture *Z*-scan techniques for determining nonlinear parameters such as absorption and refraction coefficients. All

[a]*Photonics Laboratory, Faculty of Physics, Kharazmi University, Tehran, 15719-14911, Iran*

[b]*Applied Science Research Center, Kharazmi University, Tehran, 15719-14911, Iran*

[c]*Nanotechnology Research Center, Faculty of Pharmacy, Tehran University of Medical Sciences, Tehran 1417614411, Iran*

[d]*Physical Chemistry I & Research Center of Micro and Nanochemistry and Engineering (Cμ), University of Siegen, Siegen, Germany. E-mail: majlesara@khu.ac.ir*

† Electronic supplementary information (ESI) available. See DOI: 10.1039/d0ra01380c

optical measurements have been performed at different incident powers and responses and show changes in the nonlinear behavior. The results show $NaYF_4$:Yb,Er@$NaYF_4$ is not only a nonlinear material at 980 nm but also has nonlinear properties at 532 nm.

Experimental

Materials

Lanthanide acetate hydrates such as $Y(CH_3CO_2)_3$, $Er(CH_3CO_2)_3$ (99.9%) and $Yb(CH_3CO_2)_3$ (99.9%). 1-Octadecene (90%) and oleic acid (90%) were purchased from Sigma Aldrich. Moreover, NH_4F (96%), NaOH (96%), and solvents, such as methanol, ethanol, acetone, hexane, and cyclohexane, were obtained from Merck Chemical Co. All chemicals were used as-received without further purification.

Synthesis of $NaYF_4$

18% Yb, 2% Er nanocrystals: in a typical experiment with certain modifications,[18] a solution containing acetate hydrates of Y, Yb and Er was mixed with 1-octadecene and oleic acid in a round bottom flask. The resulting mixture was then heated to 120 °C under vacuum for 30 min; after being maintained for 15 min at this temperature under a gas flow of Ar, it was cooled down to 50 °C. Subsequently, a methanol solution containing NH_4F (8 mmol) and NaOH (5 mmol) was injected into the flask, and the reaction mixture was heated at 50 °C for 30 min with stirring. After evaporating methanol by vacuum and heating at 70 °C for 15 min, the mixture was heated to 300 °C during 10 min and maintained for 1 h under a gas flow of Ar, followed by naturally cooling down to room temperature. The resulting nanocrystals were precipitated by ethanol, collected by centrifuging at 6000 rpm for 10 min, and then dispersed in hexane and washed with ethanol, followed by dispersing in hexane for the next step.

Synthesis of an epitaxial inert shell of $NaYF_4$

Yb, Er-Nanocrystals: the core@shell nanocrystals were obtained using $NaYF_4$: Yb, Er nanocrystals as seeds. $Y(CH_3CO_2)_3$ (1.8 mmol) was added to a flask containing a mixture of 1-octadecene (30 mL) and oleic acid (12 mL). The resulting mixture was heated to 120 °C under vacuum at 30 min; after that, it was maintained for 15 min under a gas flow of Ar while it was stirred and then cooled down to 80 °C. The core nanocrystals, $NaYF_4$: Yb,Er dispersed in hexane, were injected to the flask. After hexane was removed by vacuum heating the mixture, a methanol solution (20 mL) containing NaOH (4.4 mmol) and NH_4F (7 mmol) was injected to the flask and maintained at 50 °C for 30 min. Subsequently, using the abovementioned method, the core–shell nanocrystals were finally redispersed in cyclohexane.

Results and discussion

Upconversion luminescence and power dependency

The TEM image of UCNPs (Zeiss EM900 transmission electron microscope) and nanoparticle size distribution in Fig. 1a shows

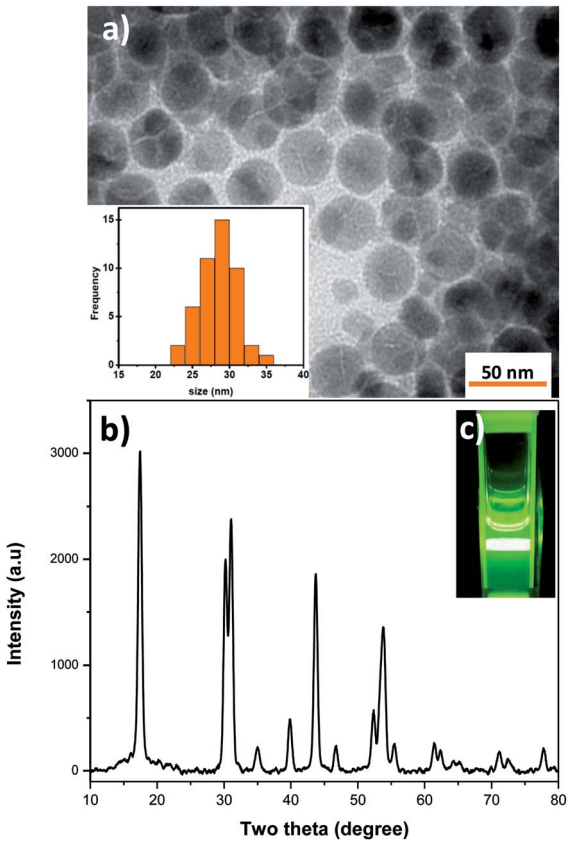

Fig. 1 (a) TEM image and distribution size of NPs, (b) XRD pattern of NPs, (c) visible PL imaging of NP colloidal suspension.

core–shell nanocrystals having an average size of 28.4 nm. The XRD pattern shown in Fig. 1b confirmed the hexagonal structure of $NaYF_4$:Yb,Er@$NaYF_4$. Moreover, the luminescence emission spectrum of the probed UCNP sample was measured

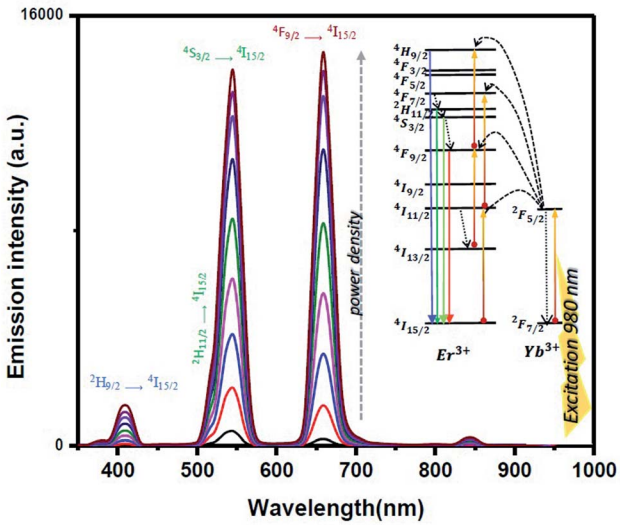

Fig. 2 PL spectra of $NaYF_4$:Yb,Er@$NaYF_4$ under excitation at 980 nm (power densities from 0.27 to 3.3 W cm^{-2}), inset shows the energy diagram of system.

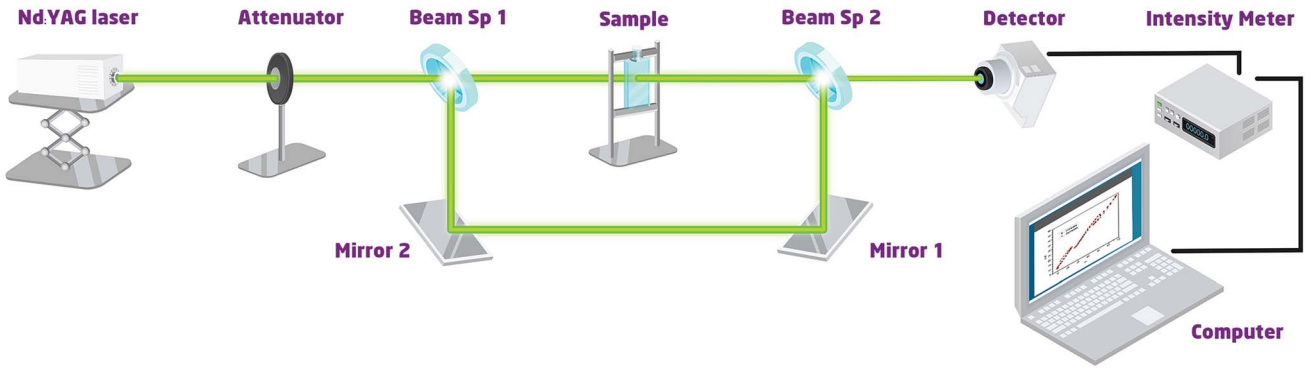

Fig. 3 Schematic of the experimental setup of Mach–Zehnder.

with a conventional photoluminescence setup. The stable colloidal dispersion of UCNPs in cyclohexane with a concentration of 10 mg mL^{-1} has been filled in a 10 mm UV-fused quartz cuvette with four transparent windows. The laser diode of 980 nm (MDL-980 from CNI Laser) was used as a CW excitation light source and a 400 μm core diameter optical fiber guided the light to the sample. A power meter (Ophire Nova II) was used for recording the excitation power; the excitation power density was calculated by the total measured power over the beam profile and the measured beam width.[19] The luminescence emission was measured at an angle of 90° to the excitation path by Avantes spectrometer (Avaspec 2048Tech) collected using a 400 μm core diameter optical fiber (Sma400-Avantes) from the cuvette (Fig. 1c).

Fig. 2 shows the upconversion luminescence spectrum and the schematic of the energy levels of Yb^{3+} as a NIR absorber and Er^{3+} as an activator and allowed energy transitions. The PL spectrum of $NaYF_4$:Yb,Er@$NaYF_4$ has two main peaks, green and red, which are related to $^4S_{3/2} \rightarrow {}^4I_{15/2}$ and $^4F_{9/2} \rightarrow {}^4I_{15/2}$ transitions.

The power dependence of emission intensity at low excitation power densities is non-linear but by increasing the excitation power densities becomes linear. This behavior is attributed due to the saturation of the upconversion processes. In this study, based on previous definitions, we focus on the low pump excitation power densities.[20,21]

To determine the number of photons responsible for the upconversion mechanism, the intensities of upconversion emissions were recorded as a function of the excitation power of 980 nm. The green and red upconversion emission intensities demonstrated quadratic power dependencies at low excitation densities, indicating two-photon upconversion mechanisms. From the log–log plot of emission intensity *versus* excitation power density (Fig. 1S†), under the low excitation power densities, the slope n for $^2H_{9/2} \rightarrow {}^4I_{15/2}$, $^4S_{3/2} \rightarrow {}^4I_{15/2}$ and $^4F_{9/2} \rightarrow {}^4I_{15/2}$ transitions is equal to the necessary photon numbers $n = 3.14$, 2.07 and 2.62 along with the increase of excitation power density; moreover, the slope n progressively reduces to $n = 2.02$, 1.17 and 1.37. This could be explained by the saturation effect, originating from the competitive process between the linear decay and UC processes consumed in the intermediate excited states. The upconversion emission intensity under pumping at 980 nm shows that the nonlinear responses depend on the excitation power density, we consider before 2 W cm^{-2} as the low-power density regime and after it as high-power density regime. For a low excitation power density regime, the green-to-red ratio is 2.2 and green intensity is more than red. By increasing the excitation power density, blue emitting energy state is feeding the red emitting energy state and leads to observe an increase in red intensity,[22] by increasing the power, green to red ratio is changed from 2.2 to less than 1.

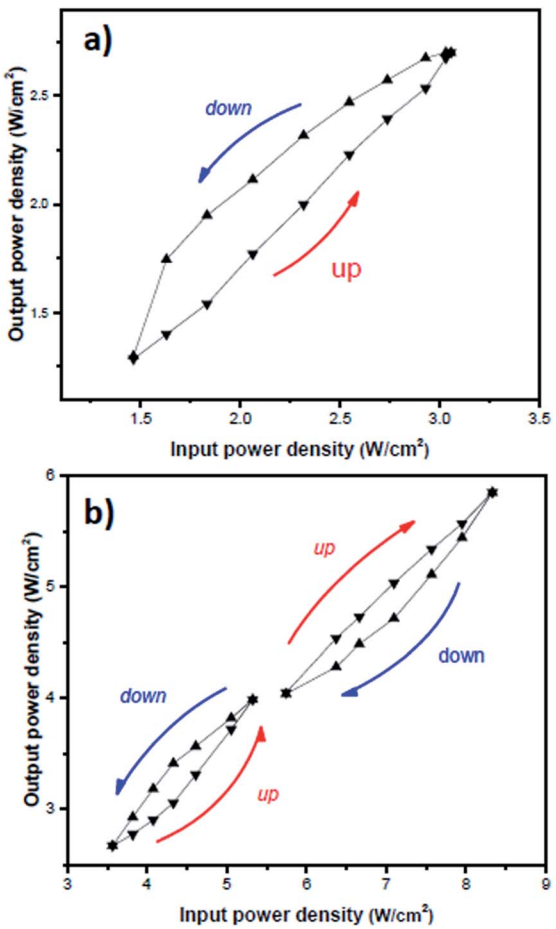

Fig. 4 Changing bistability hysteresis loops at different power densities. (a) Power densities <3 W cm^{-2}, (b) changing behaviour in power density region between 3 to 9 W cm^{-2}.

Optical bistability

The first nonlinear response, which was measured by an excitation laser of 532 nm, is optical bistability (OB). A bistable system should have two important features: nonlinearity and feedback.[23] As stated in previously reported studies,[24] some interferometers such as Mach–Zehnder (M–Z) and Fabry–Perot, with a medium that has NLO properties, can be used for observing the optical bistability loop. We have used the M–Z interferometer system because it is more efficient than other methods.[25] In a dispersive bistable sample,[26]

$$\Gamma = \frac{1}{2} + \frac{1}{2}\cos\left(\frac{2\pi d}{\lambda_0} n_2 I_0 + \phi\right) \quad (1)$$

where Γ is the normalized output power of sample, d is the length of the medium, λ_0 is the free space wavelength, φ is a constant and $n = n_0 + n_2 I_0$ is the characteristic of a Kerr medium. This nonlinear function shows bistability comprising a periodic repetition of the generic bell-shaped function.

Fig. 3 shows the experimental setup to investigate the OB. A Nd:YAG laser radiation of 300 mW at a wavelength of 532 nm was divided using a beam splitter and the required feedback for OB was achieved by mirrors (M1 and M2) and beam splitters (BS1 and BS2).

OB was measured at different power densities from 1.5 to 9 W cm^{-2} and the observed UCNP's behavior strongly depends on power density. First, as shown in Fig. 4a, the hysteresis loop was more efficient. Moreover, the close Z-scan results show that the UCNP has a higher nonlinear refraction coefficient in lower power densities, which confirms the higher gain of OB observed at lower power densities. Interestingly, a critical power density appeared by increasing the input power density. Fig. 4b shows the different OB behavior around the critical power. The rotation of hysteresis loop changes at higher powers. Moreover, the output power reduces compared to the input power. The change may originate from the saturation of fine structure levels involved in this process.

Optical phase conjugation

The next optical setup for observing nonlinear responses of UCNPs at green light is degenerate four-wave mixing (DFWM).[27] Based on the following, four coupled equations for the amplitude of four waves have been reported by solving the wave equation.[28]

$$\begin{aligned}
\frac{\mathrm{d}}{\mathrm{d}z}A_1 &= \frac{-1}{2}\Gamma\left(A_1 A_2^* + A_3 A_4^*\right)A_2/I_0 \\
\frac{\mathrm{d}}{\mathrm{d}z}A_2 &= \frac{1}{2}\Gamma^*\left(A_1^* A_2 + A_3^* A_4\right)A_1/I_0 \\
\frac{\mathrm{d}}{\mathrm{d}z}A_3 &= \frac{1}{2}\Gamma\left(A_1 A_2^* + A_3 A_4^*\right)A_4/I_0 \\
\frac{\mathrm{d}}{\mathrm{d}z}A_4 &= \frac{1}{2}\Gamma^*\left(A_1^* A_2 + A_3^* A_4\right)A_3/I_0
\end{aligned} \quad (2)$$

where A_1 and A_2 are the amplitude of forward and backward pump beams and A_3 and A_4 are the amplitude of the signal and produced OPC, respectively. These equations can be solved by considering the slowly varying amplitude approximation, the strong pump, and the boundary condition.

$$A_1(z) = \frac{\mathrm{e}^{\left(-\frac{1}{2}\Gamma z\right)} + q\,\mathrm{e}^{\left(-\frac{1}{2}\Gamma z\right)}}{1 + q\,\mathrm{e}^{\left(-\frac{1}{2}\Gamma z\right)}} A_1(0) \quad (3)$$

$$A_4^*(z) = \left(\frac{A_3^*}{A_2}\right)\frac{\mathrm{e}^{\left(-\frac{1}{2}\Gamma z\right)} - \mathrm{e}^{\left(-\frac{1}{2}\Gamma L\right)}}{1 + q\,\mathrm{e}^{\left(-\frac{1}{2}\Gamma L\right)}} A_1(0) \quad (4)$$

where Γ is the coupling constant, L is the length of sample and R is

$$R = |P|^2 = \left|\frac{A_4(0)}{A_1^*(0)}\right|^2 \quad (5)$$

With changes in the value of input power and signal, the reflectivity (R), which shows the intensity of OPC beam, will change. Experimentally, as shown in Fig. 5, the Nd:YAG laser radiation of 300 mW at a wavelength of 532 nm was divided into

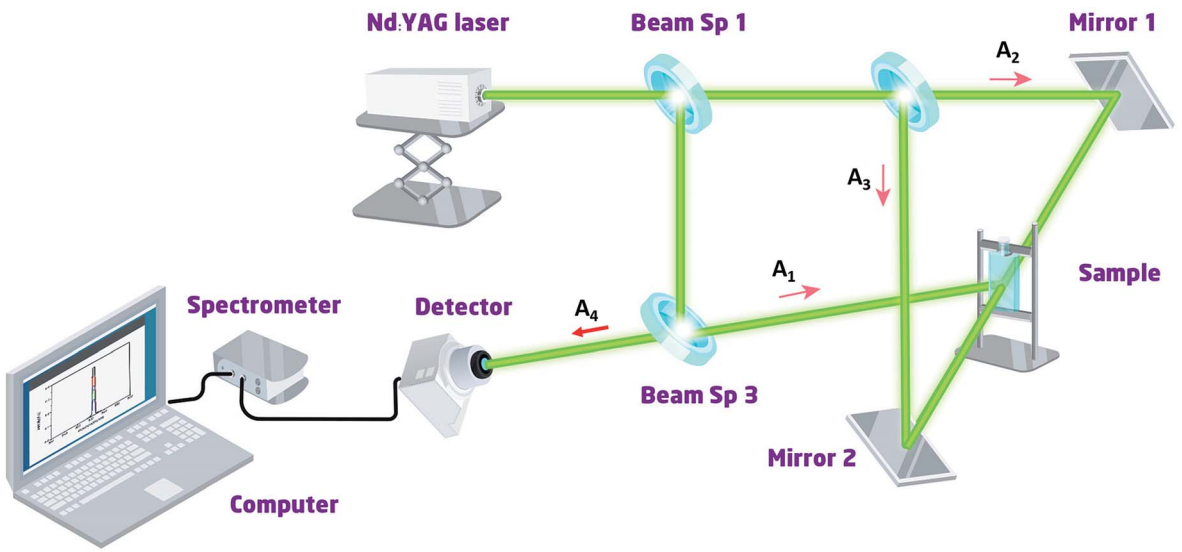

Fig. 5 Schematic of the experimental setup of degenerate four-wave mixing.

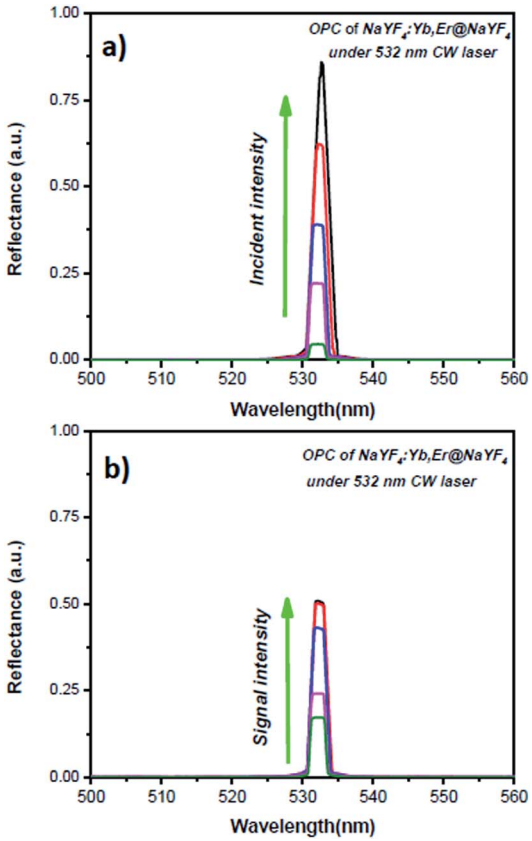

Fig. 6 Reflectivity of OPC in (a) different incident intensities, (b) different signal beam intensities.

three beams: forward pump and backward pump, two counter-propagating beams A_2 and A_3 and a signal beam A_1. The UCNPs were exposed to all of these three beams simultaneously. Using the beam splitter (BS3), the phase-conjugated wave was separated from the signal beam and detected by a photodiode detector (Thorlabs).

As stated before, the experimental results (Fig. 6a) show that by increasing the power of the incident laser beam, the reflectivity increases. Similarly, with change in the signal beam by an attenuator, the reflectivity increases (Fig. 6b), which confirms the theoretical concepts. Although the obtained reflectivity is not the same as organic materials,[29] we claim it is for the first time that OPC could be observed in UCNPs.

Z-scan technique

As mentioned, both close aperture (CA) and open aperture (OA) *Z*-scan technique were used for characterizing third-order nonlinear properties (nonlinear absorption and nonlinear refraction) of materials owing to its relative simplicity and broad variety of information that it can provide.[30] Fig. 7 shows a schematic of the implementation of close aperture *Z*-scan (CA *Z*-scan).

The sample was exposed to a Nd:YAG laser in different powers and transmission power was measured by a digital power-meter (D1) (Lab master, Coherent) placed behind the aperture and the other power-meter (D2). The detection stability, linearity dependence on light power, and dark noise are characterized by response signals of both detectors (S(D1) and S(D2)). To ensure that all possible laser fluctuations are corrected, the transmittance was calculated using the ratio

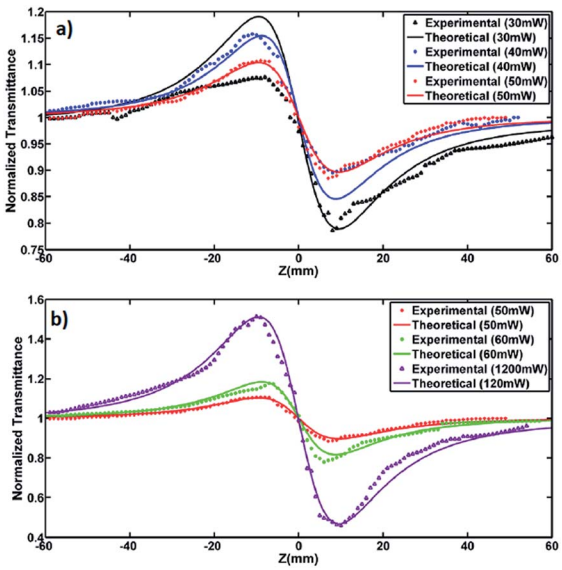

Fig. 8 Close aperture *Z*-scans (symbols) and respective theoretical fits (lines) of UCNPs at 532 nm in (a) low and (b) high regime.

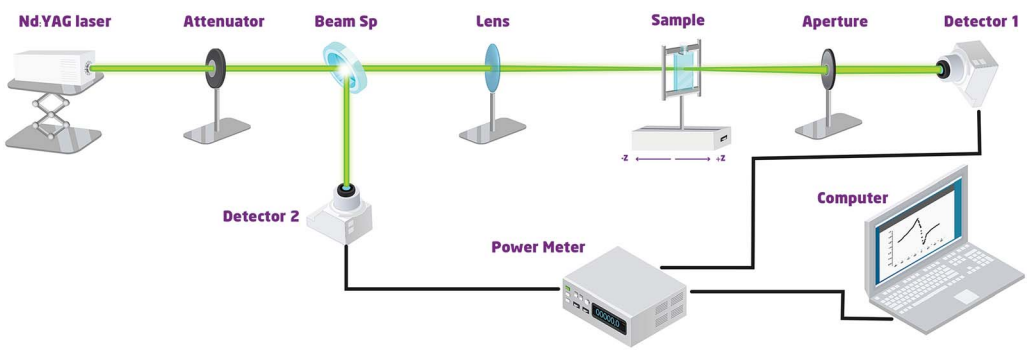

Fig. 7 Schematic of the *Z*-scan setup.

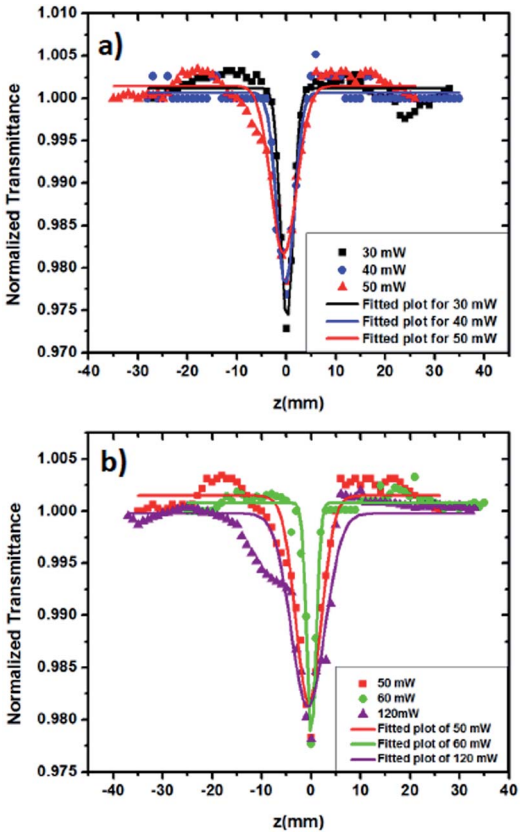

Fig. 9 Open aperture Z-scans (symbols) and respective theoretical fits (lines) of UCNPs at 532 nm in (a) low and (b) high regime.

between the signals where $g = 0.756$ is the correction factor, which ensures $T = 1$ if there is no sample loaded in the Z-scan setup. The values of the nonlinear refractive index was experimentally calculated by CA Z-scan in TEM00 Gaussian shape using eqn (6)

$$n_2 = \frac{\lambda \Delta T_{P-V}}{2\pi L_{eff}(0.406)(1-S)^{0.25} I_0} \quad (6)$$

where λ is the wavelength of light, ΔT_{P-V} changes in normalized transmittance between the peak and valley and I_0 is the intensity at the focal point. $L_{eff} = \frac{1-e^{-\alpha L}}{\alpha}$ is the effective length of cuvette where L is the sample length and α is the linear absorption coefficient obtained using Beer–Lambert's law. Moreover, $S = 1 - \exp\left(-\frac{2r_a^2}{w_a^2}\right)$ is the aperture linear transmittance, r_a is the radius of aperture and w_a denotes the beam radius of the aperture. Furthermore, the common function used for fitting the experimental data was as follows:

Table 1 Nonlinear refractive index and nonlinear absorption coefficient of $NaYF_4$:Yb,Er@$NaYF_4$ at different powers

Power (mW)	30	40	50	60	120
n_2 (cm^2 W^{-1}) $\times 10^{-8}$	8.92	7.90	6.93	9.02	10.6
β (cm W^{-1}) $\times 10^{-4}$	6.1	3.9	2.8	2.3	1.1

$$T(z) = 1 + \frac{4x\,\Delta\phi_0}{(x^2+9)(x^2+1)} \quad (7)$$

where T is again normalized transmittance; $x = z/z_0$; and $\Delta\varphi_0$ is the induced nonlinear phase shift related to the nonlinear coefficient as $\Delta\phi_0 = \frac{2\pi}{\lambda} n_2 I_0 L_{eff}$. When n_2 is positive, the sample behaves as an additional focusing lens; however, a negative n_2 causes the sample to act as if there is a defocusing lens.

As indicated in Fig. 8a, by increasing the applied power (from 30–50 mW) the NL behavior decrease due to the saturation, which it is the same as OB in this regime. Subsequently, by increasing the power to 120 MW (Fig. 8b), due to the appearance of nonradiative relaxations and thermal scattering,[31] the NL reflection increases.

After that, the OA Z-scan was applied to samples at different powers. The transmission intensity was measured without an aperture as a function of the sample position z. The nonlinear absorption coefficient can be calculated from fitting eqn (8) to the experimental data (Fig. 9):

$$T(z, s=1) = \sum_{m=0}^{\infty} \frac{\left[-\frac{\beta L_{eff} I_0}{1+\frac{z^2}{{z_0}^2}}\right]^m}{(m+1)^{\frac{3}{2}}} \quad (8)$$

where T is the normalized energy transmittance and β is the nonlinear absorption coefficient. As can be seen in Fig. 8(a) and (b) the sign of nonlinear absorption of UCNPs is positive, which indicates that two-photon absorption happened. After calculating the nonlinear absorption (Table 1), two notable points appear. First, with increase in power from 30 to 120 mW, β decreases from 6.1 to 1.1. The second point is the asymmetric behavior of CA Z-scan plot for 30 mW because of its highest nonlinear absorption coefficient rather than the other powers indicated in Table 1.

Moreover, a comparison between present results under 532 nm and the reported values at 990 nm by Nyk *et al.*[32] ($n_2 \approx 4.9 \times 10^{-15}$ cm^2 W^{-1} and $\beta \approx 1.16 \times 10^{-9}$ cm W^{-1}) have shown that values of n_2 and β at 532 nm are 7 and 5 times larger than those at 990 nm.

Conclusions

In summary, the upconversion of $NaYF_4$:Yb,Er@$NaYF_4$ was observed by photoluminescence measurement under the excitation power of 980 nm. Moreover, we reported that the $NaYF_4$:Yb,Er@$NaYF_4$ nanocrystals exhibit a strong optical nonlinearity at 532 nm. Therefore, we believe that the study of the nonlinearity of $NaYF_4$:Yb,Er at both visible and NIR wavelengths could be beneficial and applicable for fabricating multifunctional photonic devices.

Conflicts of interest

The authors declare no conflict of interest.

Acknowledgements

The authors are grateful to Dr Somayeh Salmani for help and valuable discussions in preparing this manuscript.

References

1 K. Rottwitt and P. Tidemand-Lichtenberg, *Nonlinear Optics: Principles and Applications*, CRC Press, 2014.
2 A. J. C. Kuehne and M. C. Gather, *Chem. Rev.*, 2016, **116**, 12823–12864.
3 G. Chen, H. Ågren, Y. Ohulchanskyy, P. N. Prasad, H. Agren, T. Y. Ohulchanskyy and P. N. Prasad, *Chem. Soc. Rev.*, 2015, **44**, 1680–1713.
4 N. M. Idris, M. K. G. Jayakumar, A. Bansal and Y. Zhang, *Chem. Soc. Rev.*, 2015, **44**, 1449–1478.
5 X. Liu, R. Deng, Y. Zhang, Y. Wang, H. Chang, L. Huang and X. Liu, *Chem. Soc. Rev.*, 2015, **44**, 1479–1508.
6 F. Auzel, *Chem. Rev.*, 2004, **104**, 139–173.
7 A. Nadort, J. Zhao and E. M. Goldys, *Nanoscale*, 2016, **8**, 13099–13130.
8 M. Haase and H. Schäfer, *Angew. Chem., Int. Ed.*, 2011, **50**, 5808–5829.
9 A. Fernandez-Bravo, K. Yao, E. S. Barnard, N. J. Borys, E. S. Levy, B. Tian, C. A. Tajon, L. Moretti, M. V. Altoe, S. Aloni, K. Beketayev, F. Scotognella, B. E. Cohen, E. M. Chan and P. J. Schuck, *Nat. Nanotechnol.*, 2018, **13**, 572–577.
10 F. Kaboli, N. Ghazyani, M. Riahi, H. Zare-Behtash, M. H. Majles Ara and E. Heydari, *ACS Appl. Nano Mater.*, 2019, **2**, 3590–3596.
11 P. Dawson and M. Romanowski, *J. Am. Chem. Soc.*, 2018, **140**, 5714–5718.
12 M. Sun, H. Dong, A. W. Dougherty, Q. Lu, D. Peng, W.-T. Wong, B. Huang, L.-D. Sun and C.-H. Yan, *Nano Energy*, 2019, **56**, 473–481.
13 K. Prorok, M. Olk, M. Skowicki, A. Kowalczyk, A. Kotulska, T. Lipiński and A. Bednarkiewicz, *Nanoscale Adv.*, 2019, **1**, 3463–3473.
14 Z. Li, H. Yuan, W. Yuan, Q. Su and F. Li, *Coord. Chem. Rev.*, 2018, **354**, 155–168.
15 H. Liu, C. T. Xu, D. Lindgren, H. Xie, D. Thomas, C. Gundlach and S. A. Engels, *Nanoscale*, 2013, **5**, 4770–4775.
16 G. S. Maciel and N. Rakovb, *RSC Adv.*, 2015, **5**, 17283–17295.
17 Yu Wang, L. Tu, J. Zhao, Y. Sun, X. Kong and H. Zhang, *J. Phys. Chem. C*, 2009, **113**(17), 7164–7169.
18 S. Fischer, J. K. Swabeck and A. P. Alivisatos, *J. Am. Chem. Soc.*, 2017, **139**, 12325–12332.
19 M. Mousavi, B. Thomasson, M. Li, M. Kraft, C. Wurth, U. Resch-Genger and S. Andersson-Engels, *Phys. Chem. Chem. Phys.*, 2017, **19**, 22016–22022.
20 J. C. Boyer, L. A. Cuccia and J. A. Capobianco, *Nano Lett.*, 2007, **7**, 847–852.
21 S. Heer, K. Kömpe, H. U. Güdel and M. Haase, *Adv. Mater.*, 2004, **16**, 2102–2105.
22 M. T. Berry and P. S. May, *J. Phys. Chem. A*, 2015, **119**, 9805–9811.
23 R. W. Boyd and D. Prato, *Nonlinear Optics*, Elsevier Science, 2008.
24 H. Rezig and G. Vitrant, *Opt. Commun.*, 2001, **200**, 261–269.
25 S. Salmani, E. Safari, M. H. Majles Ara and M. S. Zakerhamidi, *Opt. Mater.*, 2013, **35**, 1619–1622.
26 B. E. A. Saleh and M. C. Teich, *Fundamentals of Photonics*, Wiley, 2007.
27 S. Salmani, E. Safari, M. H. Majles Ara and M. S. Zakerhamidi, *J. Mol. Liq.*, 2013, **182**, 102–105.
28 A. Yariv and T. L. Koch, *Opt. Lett.*, 1982, **7**, 113.
29 S. Liu, W. L. Wang, C. C. Fang, T.-H. Huang and C. C. Hsu, *J. Appl. Phys.*, 2005, **97**, 013103.
30 M. Sheik-Bahae, A. A. Said, T.-H. Wei, D. J. Hagan and E. W. Van Stryland, *IEEE J. Quantum Electron.*, 1990, **26**, 760–769.
31 P. Sankar and R. Philip, *Characterization of Nanomaterials*, Woodhead, 2018, pp. 301–334.
32 M. Nyk, D. Wawrzynczyk, K. Parjaszewski and M. Samoc, *J. Phys. Chem. C*, 2011, **115**, 16849–16855.

